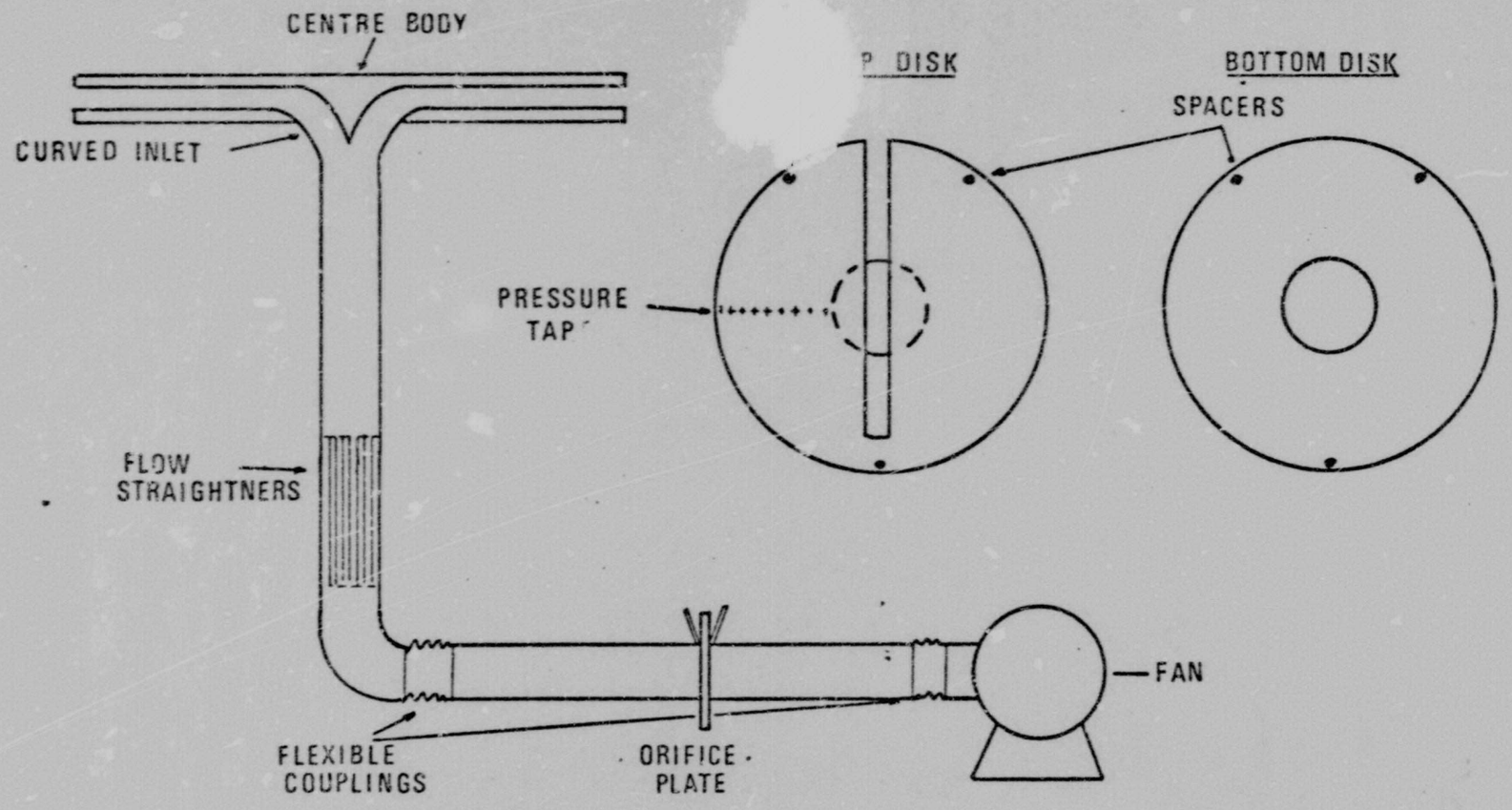

Figure 8 - Detailed schematic of flow systems

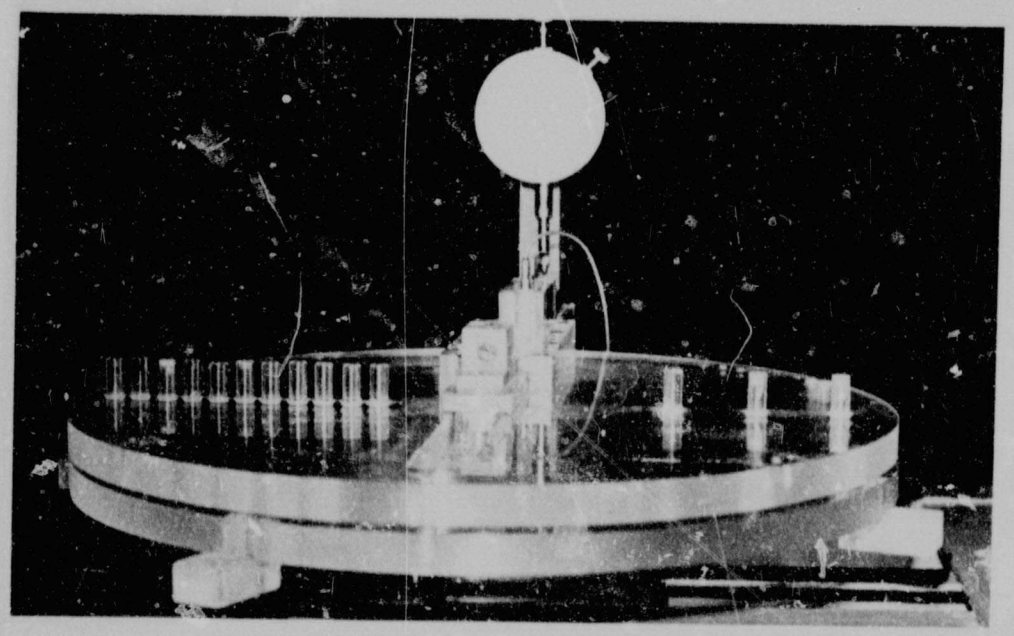

Fig. 9 - The parallel disks

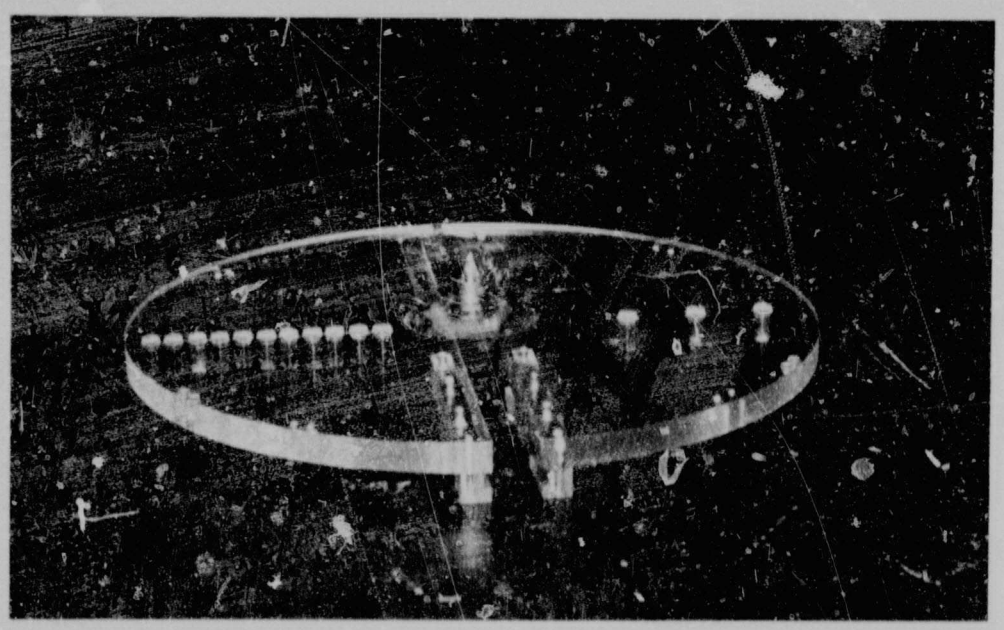

Fig. 10 - The centre body

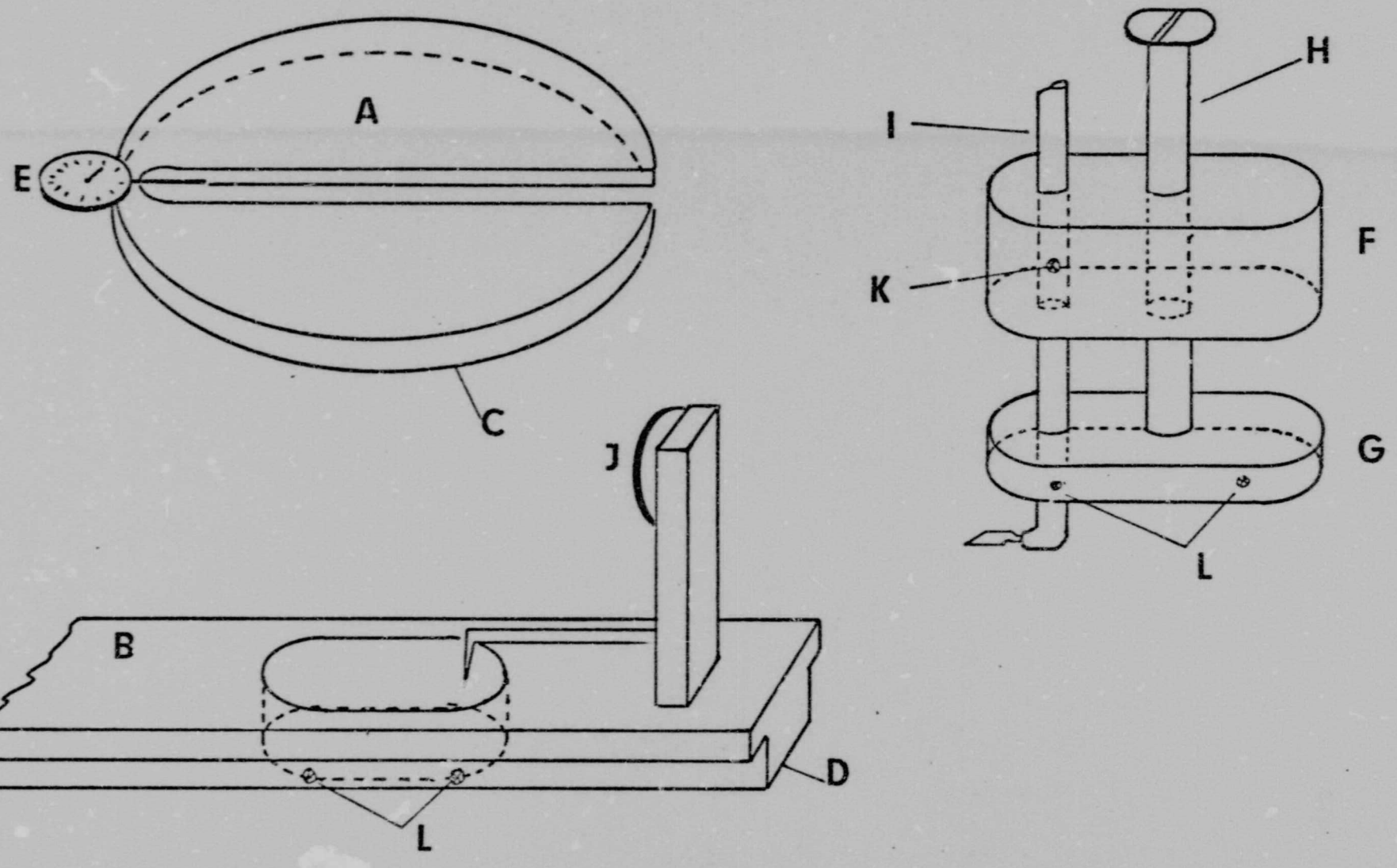

Fig. 11 - Block diagram of circuit

A hole sufficiently large to take the stem of a hot-wire probe (I) was drilled through both blocks. The stem of the hot wire was attached to block (F) by means of screw (K). Both blocks fitted into a hole in the slide and the bottom block (G) was then secured to the slide by means of screws (L). By rotating the screw (H) the top block as well as the hot-wire probe moved relative to the surface of the disk. The vertical movement of the top block was measured with a micro-dial gauge (J) which was attached to the slide. To measure the radial position of the slide another micro-dial gauge (E) was attached to the top disk with its plunger resting on the slide. To seal off the gap which appeared when the slide moved in a radial direction a perspex sheet 0,01mm thick, 90mm long and 22mm wide was glued onto the bottom surface of the disk.

4.2 INSTRUMENTATION

a) The Anemometer

A DISA 55D01 hot-wire anemometer was used in the constant temperature mode. For maximum accuracy it was necessary for the bridge to be in balance and this was achieved by applying a 300 Hz square wave signal to the bridge top and then optimising the bandwidth and gain of the servo amplifier. Since the optimum value was dependent on the probe characteristics, operating temperature, flow velocity etc., it was necessary to carry out this procedure every time a new probe was used or when the flow conditions were changed. The frequency response was in any event flat up to 10 kHz.

b) Hot-wire Probes

In this study gold plated hot-wire probes were used. They were DISA type 55P04 probes with a total wire length of 3mm and a sensor length of 1,25mm. The sensors were platinum plated tungsten while the wire ends were plated with gold. The probe was mounted in the traversing mechanism such that the sensor was perpendicular to the flow direction as shown in Figure 11.

In this geometry the probe would be cooled by the mean radial velocity as well as any transverse velocity component. However since the gap width was so narrow, i.e. 5mm, the contribution from the transverse component was negligible in comparison with the radial component and was therefore neglected.

c) Hot-wire Signal Processing

A block diagram of the circuit is shown in Figure 12. To make processing of the signal easier a lineariser was incorporated into the circuit. This is basically an electronic analog computer which simplifies the non-linear response equation for the hot wire to

$$V_{LIN} = KU_{eff} \qquad (4\text{-}1)$$

where V_{LIN} in the output voltage from the lineariser and U_{eff} is the effective cooling velocity; K is a proportionality constant determined from the calibration. The lineariser was a DISA 55D10 with a frequency response curve flat up to 10 kHz. To eliminate any high frequency noise and the d.c. component of the signal, the output from the lineariser was fed into a DISA 55D25 auxiliary unit. This unit consists of a set of adjustable high-pass and low-pass filters. The low-pass filter was set at 10 kHz while the high pass was set so that only the d.c. component of signal was eliminated.

To measure the turbulent intensity, the signal from the auxiliary unit which now only consisted of the a.c. component, was fed into a DISA 55D35 R.M.S. voltmeter. This voltmeter measured the true R.M.S. value based on the following definition

$$V_{RMS} = \sqrt{\frac{1}{T}\int_0^T V^2 dt} \qquad (4\text{-}2)$$

The integrating time constant T was variable and depending on the turbulent intensity was adjustable from 1 to 30 seconds.

The mean fluid velocity was measured directly from the output of the lineariser using a Hewlett-Packard 2212A voltage to frequency converter and a Hewlett-Packard 5312B frequency counter. By incorporating an external clock into the frequency counter's circuit it was possible to integrate the voltage over any required period. To ensure that no spurious signals were measured an oscilloscope was also connected to the lineariser output. This was also useful for determining whether the lineariser was out of range or not, e.g. the appearance of a 'chopped' output signal.

A Hewlett-Packard 3580A spectrum analyser was used to make a frequency analysis of the turbulent signal. The analyser had a variable bandwidth as well as a variable scan speed which enabled various types of signal to be analysed optimally. Since the output of the analyser gave a log-linear plot of the spectrum and it was convenient to have a

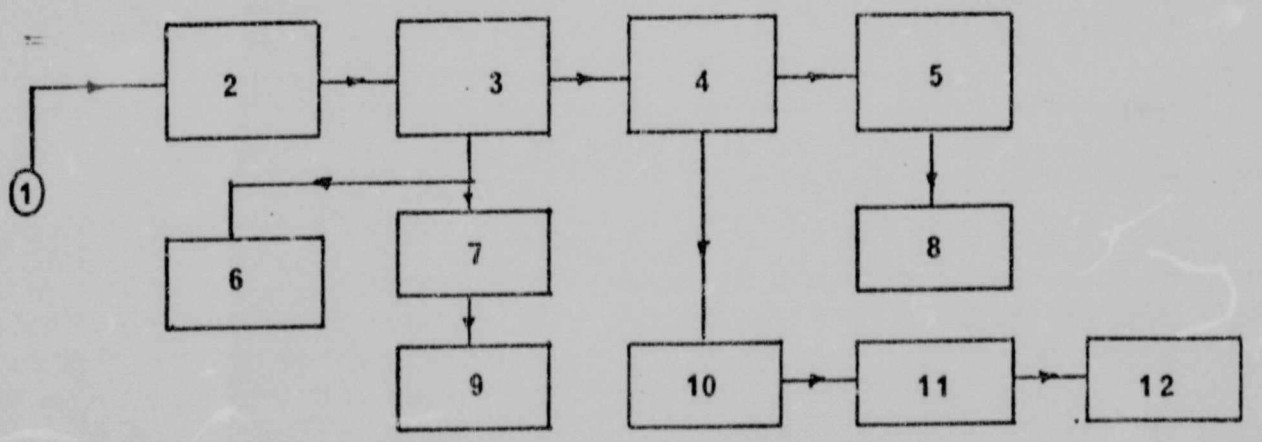

1 hot wire
2 anemometer
3 lineariser
4 auxiliary unit
5 R.M.S. unit
6 oscilloscope
7 digital voltmeter
8 digital voltmeter
9 integrating clock
10 spectrum analyser
11 logarithmic converter
12 x-y plotter

Fig. 12 - Block diagram of circuit

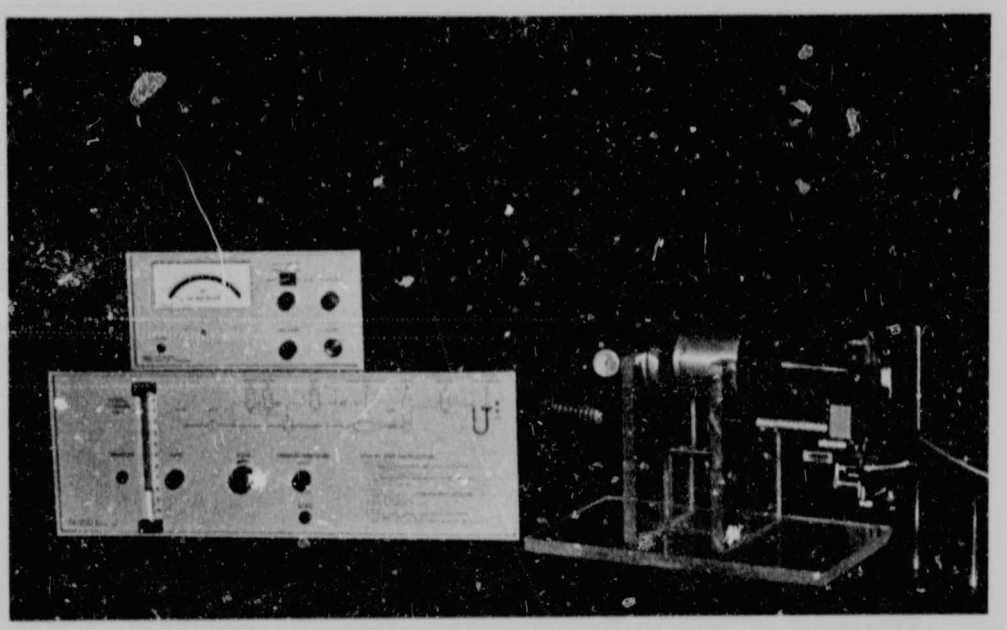

Fig. 13 - Calibration rig

log-log plot, a Hewlett-Packard 7562A logarithmic voltage converter was connected in series with one of the voltage outputs before being fed into the x - y plotter. This gave a log-log plot of the power spectrum for the longitudinal turbulent fluctuations.

4.3 EXPERIMENTAL PROCEDURE

a) Type of Measurements

Mean velocity profiles, turbulence intensity profiles and turbulent energy spectra were measured at various radial positions with varying gap width and rates of source flow. The radial pressure distribution was also measured for various flow rates.

b) Hot-wire Calibration

A general view of the DISA 55090 calibration rig is shown in Figure 13. The rig was initially calibrated against a pitot-static probe which was placed in the free jet emerging from the convergent nozzle. The turbulence level of the jet was less than 2%. Table 2 gives an indication of the accuracy of the rig.

Table 2 - Accuracy of the calibration rig

Pitot Static Velocity m/s	Calibration Rig Velocity m/s
39,6	40,00
21,10	21,2
16,73	16,81
15,93	16,02
11,35	11,11
8,21	8,13
2,34	2,29

The calibration rig velocities in Table 2 were determined from the manufacturer's design equation which is given in the instruction manual. To eliminate any effect of free convection and interference from the probe supports, the hot-wire probe was calibrated in the same orientation as it was used.

To calibrate the probe use was made of the well-known heat transfer function for the hot wire which can be expressed as

$$V^2 = A + BU_{eff}^n \qquad (4\text{-}3)$$

where V is the output voltage from the anemometer and U_{eff} is the effective cooling velocity. A and B are functions of the wire temperature and the ambient temperature. Since the anemometer was used in the constant temperature mode and the calibration rig as well as the experimental apparatus were housed in a constant temperature room, A and B were regarded as constants. The standard procedure for determining A and B is to choose a value for the exponent n, usually in the range 0,4-0,5 (King (1914) suggests that $n = 0,5$ while Collis and Williams (1959) suggest 0,45) and then apply some form of regression analysis to find the value of the constants, A and B, that best fit the data. However, it turns out that n is not a constant but a function of the mean velocity and to take this effect into account various authors, Kjellström and Hedberg (1970), Elsner and Grundlach (1973) and Davies (1968) have modified the heat transfer equation by introducing some dependency of n on the mean velocity.

However, this effect, as pointed out by Elsner and Grundlach (1973), is negligible at low velocities, i.e. $U < 25$m/sec, and under these conditions n can be regarded as a constant. In this study the mean velocity varied from 0-10m/s and therefore for calibration purposes equation (4-3) was assumed to hold. A non-linear regression analysis was then used to determine the regression coefficients A, B and n in equation (4-3). This procedure, unlike others where n is assigned some value, enabled equation (4-3) to 'be fitted' very accurately to the data. In Table 3 and Figure 14 we list some results of a typical probe calibration.

Perry and Morrison (1971) have pointed out that the above static calibration method can result in errors of up to 20 percent when measuring turbulent quantities. However, this only occurs when high mean velocities are encountered and equation (4-3) becomes then inadequate because of the dependence of n on the mean velocity.

In order to obtain good linearisation of the anemometer output voltage with the DISA 55D10 linearisers, the constants A, B and n in (4-3) must be accurately known. (These constants are used to set up the different analog circuits in the linearisers.) The regression analysis in fact gives us these constants and in Table 4 we compare the linearised velocity with the actual fluid velocity.

Table 3 - Hot-wire calibration

U (m/s)	Measured V^2 (volts)	Calculated V^2 (volts)	% difference
10,1816	18,7359	18,7007	0,188
9,7640	18,5003	18,4763	0,129
9,4404	18,3029	18,2988	0,023
8,9707	18,0251	18,0351	-0,056
8,7517	17,8903	17,9095	-0,107
7,5720	17,1818	17,2018	-0,117
6,9979	16,8116	16,8355	-0,142
6,5490	16,5250	16,5375	-0,076
6,0584	16,1941	16,1987	-0,028
4,7641	15,2357	15,2254	0,068
4,2839	14,8471	14,8278	0,130
3,8559	14,4734	14,4524	0,145
3,13574	13,7819	13,7651	0,122
2,2484	12,7834	12,7861	-0,021
1,7892	12,1710	12,1942	-0,191
1,6148	11,8109	11,7888	0,187
1,4060	11,4704	11,4751	-0,041
1,1503	11,0297	11,0550	-0,230
0,7321	10,3142	10,3073	0,060

Sum of squared errors = 0,005663
R.M.S. error = 0,01825
Average error = 0,01609
Best parameter values
A = 6,7739 B = 4,1638 n = 0,4535

Table 4 - Accuracy of the lineariser

V (volts) from lineariser	U (m/s) from lineariser	U(m/s) from calibration rig
10,004	10,56	10,56
8,549	9,03	9,05
6,855	7,23	7,24
4,745	5,01	4,95
2,990	3,16	3,10
1,400	1,48	1,42

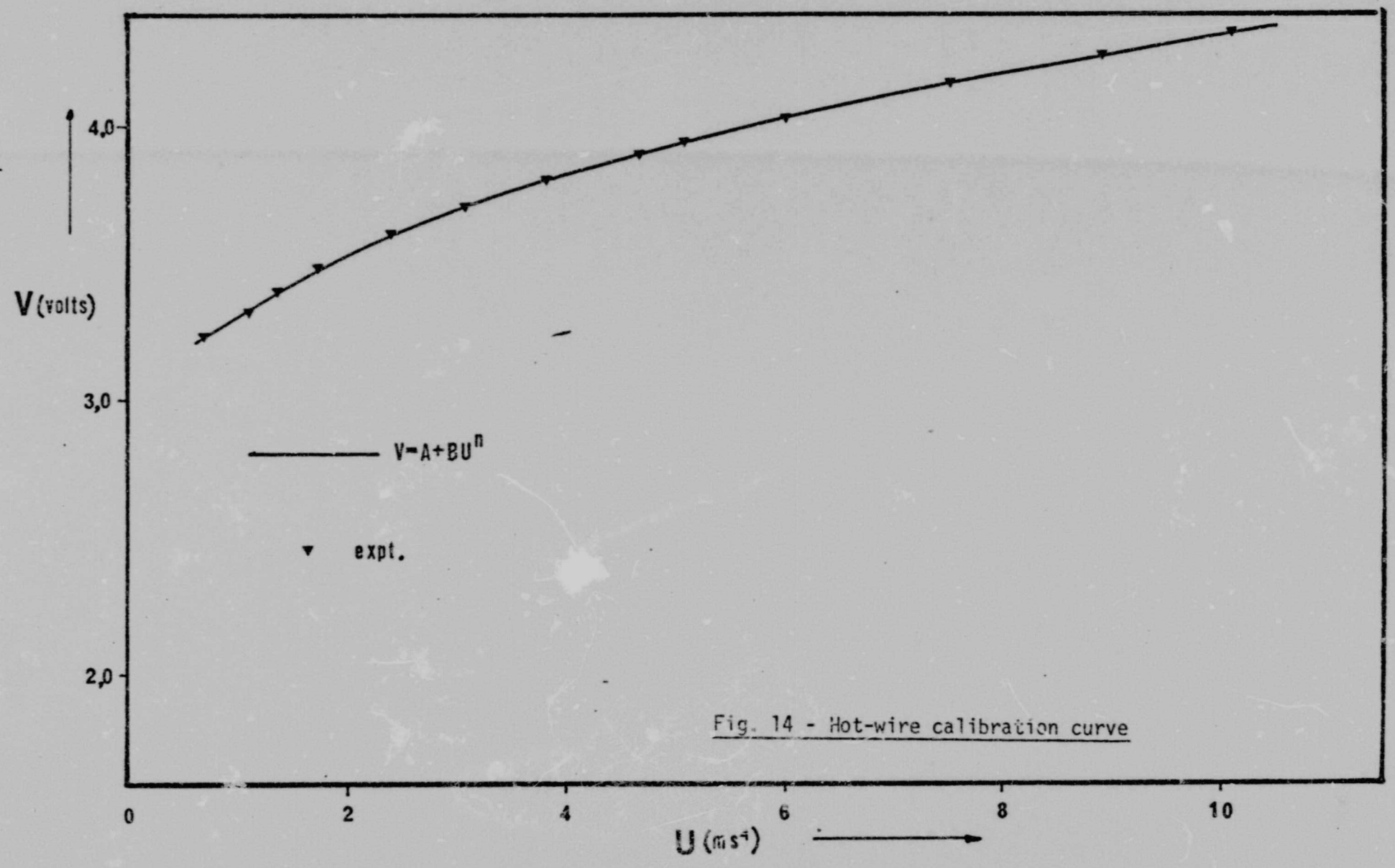

Fig. 14 - Hot-wire calibration curve

c) Flow Separation and Symmetry

To determine the effectiveness of the centre body and the curve inlet on eliminating separation, a simple flow visualisation technique was employed. With the aid of a smoke generator, cigarette smoke was introduced into the supply pipe just below the bottom disk. A collimated light beam was then shone between the disks and by observing at right angles to the beam it was possible to determine whether flow separation had taken place or not. It was found that the degree of separation was determined by the gap width and the volumetric flow rate. In this study the gap width was never larger than 5mm and for the range of flow rates investigated flow separation did not take place.

The 90° bend in the supply pipe tended to induce secondary flow patterns which resulted in an asymmetrical velocity profile at the entrance of the disks and subsequently an asymmetrical flow pattern between the disks. This was eliminated by placing drinking straws into the supply pipe after the 90° bend. In Figure 15 a velocity traverse is shown across the entrance of the supply pipe with and without drinking straws. To check on the angular symmetry of the flow a hot-wire probe was placed at various positions on the perimeter of the disks and the mean velocity measured. The results are given in Table 5.

Table 5 - Flow symmetry

Angular position of probe	U (m/s)
0°	4,87
45°	4,81
90°	4,78
135°	4,83
180°	4,86
225°	4,85
275°	4,79
315°	4,85

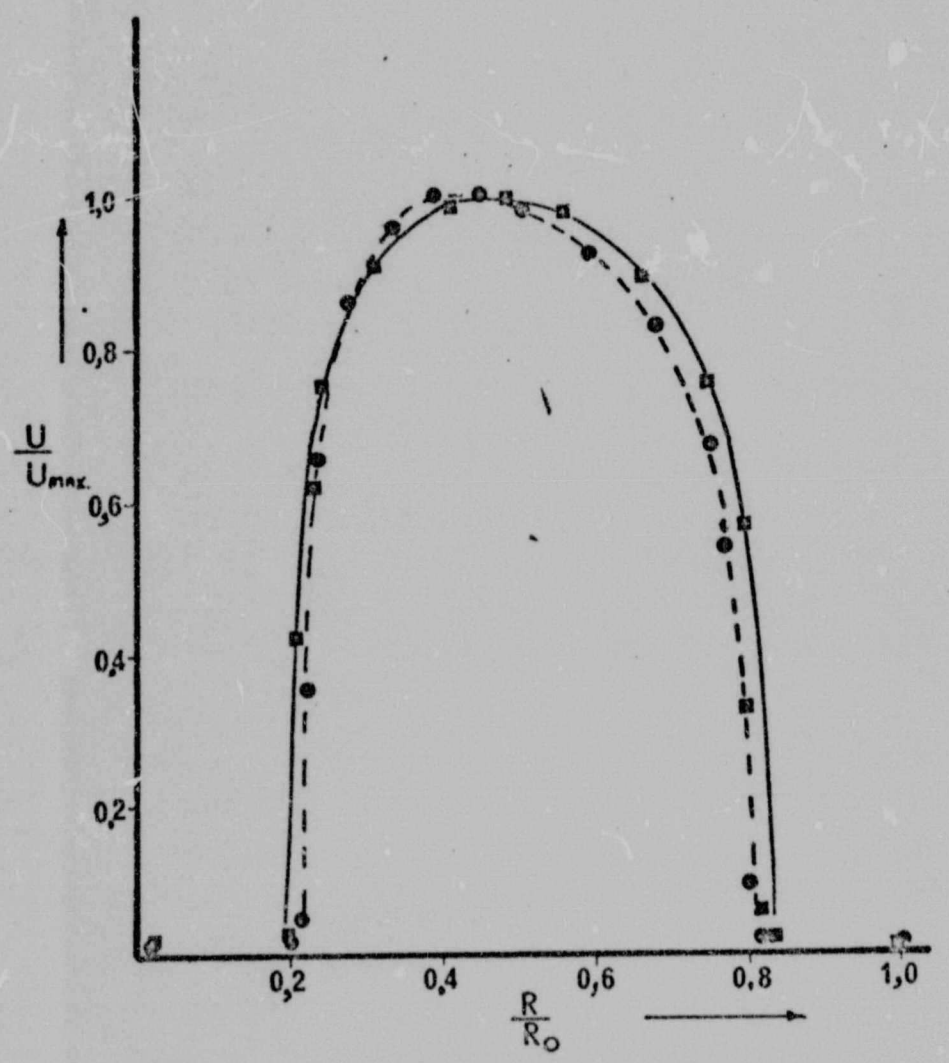

velocity profile with flow straighteners

velocity profile without flow straighteners

R_o = diameter of the rounded entrance

Fig. 15 - Velocity traverses across the entrance of the channel.

d) Measurement of Mean Velocity and Turbulent Profiles

Before any turbulent or velocity measurements could be made the hot-wire probe had to be positioned in the slide. This was achieved by mounting the slide on a stand attached to a travelling microscope. Once the exact position of the probe wire relative to the slide surface had been measured, the micro-dial gauge on the slide was set to zero. To check on the accuracy of the traversing mechanism the traversing screw was then rotated a number of turns and the distance of the probe from the slide surface measured with the travelling microscope. It was found to be accurate to ±0,05mm. (Note: the micro-dial gauge was graduated in intervals of 0,01mm.) The radial micro-dial gauge was set to zero by positioning the slide in the slot such that the probe wire was aligned with the outer periphery of the disk. This was achieved using a cathetometer.

To determine the effect of the solid boundary on the rate of heat loss from the probe, the output voltage from the lineariser was recorded as the probe approached the surface of slide in still air. At 0,25mm from the surface of the slide, (this was the closest reading made) the output voltage corresponded to 0,05m/s which was in most cases approximately 10 percent of the mean velocity. Although Wills (1962) gives a method for correcting voltage readings it is not very satisfactory because it is based on specific laminar flow conditions. Therefore the best correction that could be made was to rezero, in still air, the lineariser output voltage when the probe was 0,25mm from the slide surface.

After completing the above preliminaries, velocity and turbulent measurements could be made. The centrifugal fan was started up and once the pressure drop across the orifice plate was constant, the traversing screw was rotated and the reading on the micro-dial gauge noted. (At any one radial position up to 10 readings were taken across one half of the disk gap.) Depending on the turbulence intensity the output from the lineariser was integrated over some time period and the mean voltage recorded. In most cases the time period was 10 seconds but up to 100 seconds had to be used when the turbulent intensity was of the order of 0,25. At the same time the root-mean-square value of the turbulent signal was measured on the DISA 55D35 R.M.S. unit with a time constant sufficiently large to give a steady reading.

To convert the voltage readings to velocities the readings were multiplied by the lineariser calibration constant K, defined by eqn. (4-1). After every run the probe was recalibrated to eliminate any drift due to dirt accumulation on the wire and aging of the probe.

e) Measurement of Turbulent Spectra

A spectrum analysis of the turbulent signal was made by connecting the lineariser output to spectrum analyser input. The spectra were measured at various radial and transverse positions in conjunction with the mean velocity and turbulent intensity at these points. The frequency span was set at 20 kHz while the resolution bandwidth was set at 30Hz. Because of the slow response of the x-y plotter in comparison with the spectrum analyser, the sweep time was varied over the frequency range. At low frequency a sweep time of 200 secs per 2kHz was used and then steadily increased to 5 secs per 2kHz.

f) Static Pressure Measurements

An inclined manometer which had a resolution of 0,005mm of water was used to measure the radial pressure distribution. This method was adequate at high flow rates but at low flow rates the radial pressure drop became too low for the manometer and the readings were used only as a qualitative guide.

g) Accuracy of the Mean Velocity Profiles

Although the accuracy of the calibration unit was known the effect of measuring a velocity profile between such a narrow gap width was unknown. To determine the accuracy of the velocity profile, the profile was numerically integrated using Simpson's rule and the volumetric flow rate determined. This flow rate was then checked against the orifice plate calculations and it was found that the profiles gave a volumetric flow rate not more than 8% higher than the orifice plate.

4.4 RESULTS AND DISCUSSION

a) Mean Velocity Profiles and Pressure Distributions

In this study the range of Reynolds numbers, Re, were such that the experiments were either in the fully turbulent region or else in some transitional region; the lower limit of the Reynolds number being determined by the hot-wire calibration unit. Below an average velocity of 1m/s the calibration of the hot-wire became impractical.

In Figures 16 to 20 we have plotted the mean velocity profiles for various Reynolds numbers with the gap width fixed at 5,0mm. The velocity has been normalised with respect to the centre-line velocity, U_c, while the transverse co-ordinate, z, has been normalised with respect to half the gap width, h. For comparison we have also plotted the laminar parabolic profile given by equation (2-16). The velocity profiles become progressively more parabolic with increasing radius. Near the centre of the disks the profiles are not symmetric with respect to the centre line of the channel, i.e. $\frac{U}{U_c} > 1$. This is due to the centre body which causes the flow to spread at the entrance like a radial wall jet with the maximum velocity near the top disk.

In Figure 21 we have examined the effect of reducing the gap width from 5,0mm to 3,8mm. Although the Reynolds number has remained approximately the same as in Figure 20, the velocity profiles are more symmetric. This is to be expected because by reducing the gap width the radial co-ordinate is effectively increased and subsequently the flow has more chance to develop.

In Figure 22 the dimensionless radial pressure distribution

$$P_D = \frac{(P-P_\infty)(2h)^4}{\frac{1}{2}\rho Q^2} \qquad (4\text{-}4)$$

has been plotted against $\hat{r}$ for various values of the Reynolds number. The gap width, 2h, was fixed at 5,0mm. In terms of these co-ordinates the distributions very nearly collapse onto one curve suggesting that they are insensitive to changes in Re. Moller (1963) noticed similar trends but at very much higher Reynolds numbers.

b) Turbulent Measurements

The variation in turbulent intensity across the channel at various downstream radii and Reynolds numbers are shown in Figures 23 to 25. The profiles were measured at the same time as the mean velocity profiles in Figures 16 to 21. In Figures 23 and 24 the turbulent intensity decreases with increasing radius and the position of the maximum value of

$$\sqrt{\frac{\overline{u^2}}{U_c}}$$

moves towards the centre of the channel. Figure 29 shows that during this decay the maximum value of $\overline{u^2}$ exhibits exponential decay with respect to $\hat{r}$ and the decay rate appears to be a function of the Reynolds number. These trends are similar to those noticed by Laufer (1962)

and Badri Narayanan (1968) during their investigation of reverse transition in pipe and channel flows. At higher Reynolds numbers the turbulent intensity shown in Figures 25 to 28 increases with increasing radius. This effect can be explained by inspecting various terms in the turbulent energy equation. The turbulent production term in the turbulent energy equation can be written as

$$\text{Prod} = -\{\overline{uv}\frac{\partial U}{\partial z} + (\overline{u^2} - \overline{v^2})\frac{\partial U}{\partial r} + (\overline{w^2} - \overline{v^2})\frac{U}{r}\} \qquad (4\text{-}5)$$

where $\overline{w^2}$ is the turbulent fluctuating component in the tangential direction. As there is no mean flow in the tangential direction and the gap width is very small, the magnitude of $(\overline{w^2} - \overline{v^2})$ will be close to zero. Also as $\overline{u^2}$ is very much larger than $\overline{v^2}$ (4-5) can be simplified to

$$\text{Prod} = -\{\overline{uv}\,\frac{\partial U}{\partial z} + \overline{u^2}\,\frac{\partial U}{\partial r}\} \qquad (4\text{-}6)$$

The production of turbulence in the radial direction is $-\overline{u^2}\frac{\partial U}{\partial r}$ and as $\frac{\partial U}{\partial r}$ is negati the turbulent energy in the radial direction will increase when low decelerates. However at low flow rates and large $\hat{r}$, $\frac{\partial U}{\partial r}$ be negligible indicating no net production of turbulence in the radial direction. When this occurs the turbulence will decay in the radial direction.

c) Turbulent Spectrum

The spectral distributions of $\overline{u^2}$ were measured along the centre line of the channel for a range of Reynolds numbers and are shown in Figures 30 to 33. Examining these spectral distributions a certain similarity can be noticed. That is to say there appears to be some length scale characteristic of the decay process.

By defining a length scale Λ such that

$$\frac{UE(0)}{\Lambda\overline{u^2}} = 4 \qquad (4\text{-}7)$$

where $E(0)$ is the value of the spectrum at zero frequency, the spectral distributions for a fixed Re can indeed be collapsed onto one curve. These curves for the various Re are shown in Figures 34 to 37. This trend has also been noticed by Laufer (1962), Sibulkin (1962) and Badri Narayanan (1968). It should be pointed out that the length scale Λ